Segmentation Of Infant Brain MR Images Based On Adaptive Shape Prior And Higher-order MGRF

M. Ismail, et al.

IEEE, 2015

NeuroSpectrum Insights, Inc.
info@neurospectruminsights.com
www.neurospectruminsights.com

SEGMENTATION OF INFANT BRAIN MR IMAGES BASED ON ADAPTIVE SHAPE PRIOR AND HIGHER-ORDER MGRF

M. Ismail[1],*M. Mostapha*[1], *A. Soliman*[1],*M. Nitzken*[1], *F. Khalifa*[1],
A. Elnakib[1], *G.Gimel'farb*[2], *M. F. Casanova*[3], *and A. El-Baz*[1]
[1]BioImaging Laboratory, Bioengineering Department, University of Louisville, Louisville, KY, USA.
[2]Department of Computer Science, University of Auckland, Auckland 1142, New Zealand.
[3]Department of of Psychiatry and Behavioral Science, University of Louisville, Louisville, KY, USA.

ABSTRACT

This paper introduces a new framework for the segmentation of different brain structures from 3D infant MR brain images. The proposed segmentation framework is based on a shape prior built using a subset of co-aligned training images that is adapted during the segmentation process based on higher-order visual appearance characteristics of infant MRIs. These characteristics are described using voxel-wise image intensities and their spatial interaction features. In order to more accurately model the empirical grey level distribution of infant brain signals, a Linear Combination of Discrete Gaussians (LCDG) is used that has positive and negative components. Also to accurately account for the large inhomogeneity in infant MRIs, a higher-order Markov Gibbs Random Field (MGRF) spatial interaction model that integrates third- and fourth-order families with a traditional second-order model is proposed. The proposed approach was tested on 40 in-vivo infant 3D MR brain scans, having their ground truth created by an expert radiologist, using three metrics: the Dice coefficient, the 95-percentile modified Hausdorff distance, and the absolute brain volume difference. Experimental results promise an accurate segmentation of infant MR brain images compared to current open source segmentation tools.

Index Terms— Adaptive Shape, Higher Order MGRF, Infant Brain Segmentation

1. INTRODUCTION

Accurate segmentation of brain tissues from Magnetic Resonance Imaging (MRI) data is an essential step in clinical diagnostics, therapy evaluation, human brain mapping, and neuroscience [1, 2]. The analysis and treatment of brain injuries and disorders rely on accurate brain segmentation that accounts for classifying its different tissue types [3]. Brain MRI segmentation has many challenges, especially with infant brains, such as image noise, inhomogeneities, and low contrast between tissue types. Also infant brains have a reverse in contrast in the White Matter and Gray Matter [4], and a higher amount of noise than adult brains [5]. This is due to the fact that the WM is unmyelinated and has water makeup that results in a low contrast between tissue classes, and an intensity level that is almost identical to that of GM, which makes it difficult to distinguish these 2 classes even by experts [6].

There has been extensive work in the literature that addresses adult brain segmentation, with fewer techniques suited for infant brain segmentation. Probabilistic methods were adopted in [7] for adult brain segmentation, where a map classifier along with a probability clustering method are employed for brain tissue classification. In [8], a pairwise joint MGRF interaction model was used for adult brain segmentation, however the pairwise MGRF failed to capture large inhomogeneities of signals, and thus would not suit infant brain segmentation. Deformable models were used in [9, 10], where region-boundary models are employed to segment brain tissues. Atlas-based methods have also been adopted, as in [11, 12], where brain shape priors are registered with the subjects to be segmented to guide the segmentation process.

Since the intensity alone would fail to segment infant brain tissues due to the similar intensities of different structures and poor contrast, fewer techniques can be found for infant brain segmentation. Xue et al. [4] employed an Expectation-Maximization (EM) algorithm along with a Markov Random Field (MRF) prior for infant brain segmentation. Classifying brain structures, such as WM, CSF, central GM, and cortical GM was conducted by Abneek et al. in [13], where T2-weighted images of neonatal brains were used. Probability maps were used to segment each brain tissue class with a K-nearest neighbor classifier. Wang et al. [14] segmented T1, T2, and diffusion-weighted brain images using a sparse representation of the complementary tissue distribution. In [15], the random forest technique was used to integrate features from the different modalities for tissue segmentation along with probability maps of GM, WM, and CSF. Some approaches use longitudinal scans at a late-time-point age, where the contrast is much better between different tissue types, from which probabilistic atlases are constructed to guide segmentation of neonatal images,[16, 17]. Segmentation with shape priors was also adopted as in [18, 19, 20].

This paper proposes a novel technique for infant brain segmentation from T1-weighted images (Fig. 1). Adaptive probabilistic shape models for the shape and first-order visual appearance of MRI data are employed to initialize the segmentation. This is then combined with a novel higher-order Markov Gibbs Random Field (MGRF) spatial interaction model(up to fourth order) with analytic estimation of potentials. This joint model guarantees increasing the segmentation accuracy by accounting for the large inhomogeneities and noise in infant brain MRI data. Also the analytic estimation of potentials generalizes the proposed model to different MRI subjects, unlike the use of empirical values in most of the work present in literature which would require manual setting for each subject. The strength of the proposed algorithm lies in the fact that it neither depends on multiple modalities for acquiring images (depends only on T1-weighted images) nor on longitudinal studies which are not always available for research purposes.

2. JOINT MGRF MODEL OF INFANT MR BRAIN IMAGES

Let $\mathbf{R} = \{(x, y, z) : 0 \leq x \leq X-1, 0 \leq y \leq Y-1, 0 \leq z \leq Z-1\}$; $\mathbf{Q} = \{0, 1, \ldots, Q-1\}$; and $\mathbf{L} = \{0, 1, \ldots, L-1\}$ denote a finite 3D arithmetic lattice of the size XYZ supporting grayscale images and their region maps, a finite set of Q integer values, and a

978-1-4799-8339-1/15/$31.00 ©2015 IEEE

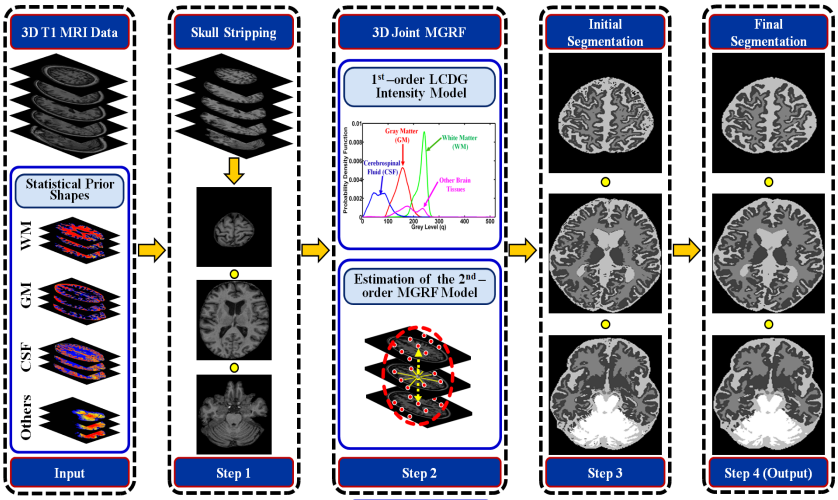

Fig. 1. Illustration of the proposed framework.

set of region labels L, respectively. Let $\mathbf{g} = \{g_{x,y,z} : (x,y,z) \in \mathbf{R};\ g_{x,y,z} \in \mathbf{Q}\}$ and $\mathbf{m} = \{m_{x,y,z} : (x,y,z) \in \mathbf{R};\ m_{x,y,z} \in \mathbf{L}\}$ be a grayscale image taking values from $\mathbf{Q}$, i.e., $\mathbf{g} : \mathbf{R} \rightarrow \mathbf{Q}$, and a region map taking values from $\mathbf{L}$, i.e. $\mathbf{m} : \mathbf{R} \rightarrow \mathbf{L}$ respectively. An input T1-weighted brain image, $\mathbf{g}$, co-aligned to the training database, and its map, $\mathbf{m}$, are described with a joint probability model: $\mathbf{P}(g,m) = \mathbf{P}(g|m)\mathbf{P}(m)$, which combines a conditional distribution of the images given the map $\mathbf{P}(g|m)$, and an unconditional probability distribution of maps $P(\mathbf{m}) = P_{\mathbf{sp}}(\mathbf{m})P_{\mathbf{V}}(\mathbf{m})$. $P_{\mathbf{sp}}(m)$ denotes a weighted shape prior, and $P_{\mathbf{V}}(m)$ is a Gibbs probability distribution with potentials $\mathbf{V}$, which specifies a MGRF model of spatially homogeneous maps ($\mathbf{m}$). The model's components are outlined below.

2.1. First-Order Intensity Model

The first-order visual appearance of each brain label is modeled by separating a mixed distribution of voxel intensities of the infant brain MRIs into individual components associated with the dominant modes of the mixture. The latter is precisely approximated with a Linear Combinations of Discrete Gaussians (LCDG) [21, 22] with positive and negative components, which is based on a modified version of the classical Expectation Maximization (EM) algorithm.

Let $\mathbf{\Psi}_\theta = (\Psi(q|\theta) : q \in \mathbf{Q})$ denote discrete Gaussian (DG) with parameters $\theta = (\mu, \sigma)$, integrating a continuous 1D Gaussian density with mean μ and variance σ^2 over successive gray level intervals. The LCDG with four dominant positive DGs and $C_p \geq 4$ positive and $C_n \geq 0$ negative subordinate DGs is [21]:

$$P_{w,\Theta}(q) = \sum_{k=1}^{C_{\mathrm{p}}} w_{p:k}\psi(q|\theta_{p:k}) - \sum_{\kappa=1}^{C_{\mathrm{n}}} w_{n:k}\psi(q|\theta_{n:k}) \qquad (1)$$

where all the weights $\mathbf{w} = [w_{\mathrm{p:k}}, w_{\mathrm{n:k}}]$ are non-negative and meet an obvious constraint $\sum_{k=1}^{C_{\mathrm{p}}} w_{p:k} - \sum_{k=1}^{C_{\mathrm{n}}} w_{n:k} = 1$. All LCDG parameters, including the DGs numbers, are estimated from the mixed empirical distribution to be modeled using the modified EM algorithm. For further details on the modified EM algorithm, please refer to [21, 23].

2.2. MGRF Model With Higher-Order Cliques

In addition to the first-order visual appearance model, the spatial interactions between the brain voxels are also taken into account. In this paper we propose a higher-order Markov Gibbs Random Field (MGRF) spatial interaction model that adds the pairwise,the triple, and the quad cliques, along with analytical estimation of the potentials. In addition to this, it is used simultaneously with shape and intensity models, not as a refinement step. As a result, the proposed approach has the ability to account for the large inhomogeneities of infant MRIs, thus reducing the noise effects and increasing the segmentation accuracy. Details of the proposed higher-order MGRF are described below.

Let $\mathbf{C}_a$ denote a family of s-order cliques of an interaction graph with nodes in the 3D lattice (x,y,z) and edges connecting the interacting, or interdependent sites, (Fig. 2). To account for large variations of infant MRIs, the label interactions are modeled by a spatially homogenous MGRF with up to fourth-order interactions over the nearest 26-neighborhood of voxels:

$$P_V(m) = \frac{1}{Z_V} exp\left(\sum_{a=1}^{A}\sum_{c\in C_{\mathrm{a}}} V_a(m(x,y,z)) : (x,y,z) \in c\right) \qquad (2)$$

where A clique families describe the geometry of the graph interactions, $\mathbf{V} = [V_a : 0,...,L] \rightarrow (-\infty,\infty) : a = 1,....,A]$ is a collection of Gibbs potential functions V_a for the families $\mathbf{C_a}$, and the partition function $\mathbf{Z_V}$ normalizes the probabilities over the parent population $\mathbf{M} = \{0,\ldots,L\}^{XYZ}$ of all maps. $\mathbf{V}$ is the Gibbs potential value, and L denotes the set of region labels. An initial region map $\mathbf{m}$, obtained by the voxel-wise classification, allows for analytically approximating the maximum likelihood estimates of the potentials and computing the voxel-wise probabilities of the region labels. For symmetry sake, only equality or inequality of the labels in clique $\mathbf{c}$ is taken into account. The second-, third-, and forth-order potentials are given by Eqs. (3), (4), and (5) respectively:

$$V_a(m_{\mathbf{p}_1}, m_{\mathbf{p}_2}) = \begin{cases} V_{2:a:\mathrm{eq}} & \text{if} \quad m_{\mathbf{p}_1} = m_{\mathbf{p}_2} \\ -V_{2:a:\mathrm{eq}} & \text{otherwise} \end{cases} \qquad (3)$$

$$V_a\left(m_{\mathbf{p}_1}, m_{\mathbf{p}_2}, m_{\mathbf{p}_3}\right) = \begin{cases} V_{3:a:\mathrm{eq}_3} & \text{if} \quad m_{\mathbf{p}_1} = m_{\mathbf{p}_2} = m_{\mathbf{p}_3} \\ -V_{3:a:\mathrm{eq}_3} & \text{otherwise} \end{cases} \qquad (4)$$

$$V_a\left(m_{\mathbf{p}_1}, m_{\mathbf{p}_2}, m_{\mathbf{p}_3}, m_{\mathbf{p}_4}\right) = \begin{cases} V_{4:a:\mathrm{eq}_4} & \text{if 4 equal labels} \\ V_{4:a:\mathrm{eq}_3} & \text{if 3 equal labels} \\ -\left(V_{4:a:\mathrm{eq}_3} + V_{4:a:\mathrm{eq}_4}\right) & \text{otherwise} \end{cases} \tag{5}$$

where $m_{\mathbf{p}_i}$ is the region map label at the voxel $\mathbf{p}_i = (x_i, y_i, z_i)$. The proposed analytical approximation of the Gibbs potentials from a given map $\mathbf{m}$ extends earlier 2D second-order MGRFs (e.g.,[[23]]) to the 3D higher-order model. Fig. 3 highlights the advantage of integrating higher order model with pairwise interactions. Brain tissues are better connected with higher order model, Fig. 3(c), than they are with only the pairwise interaction model, Fig. 3(b). This is essential for our future work of shape analysis, where the ultimate goal is to extract features from complete brain meshes in order to discriminate between autistic and control subjects.

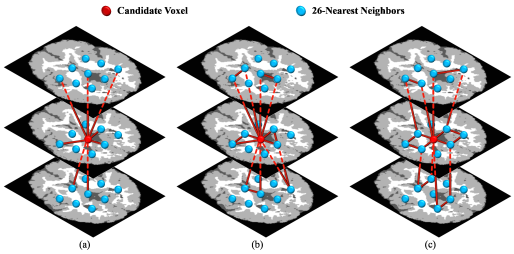

Fig. 2. Illustration of the second- (a), third- (b), and fourth-order (c) cliques of the proposed MGRF model for the 26-neighborhood.

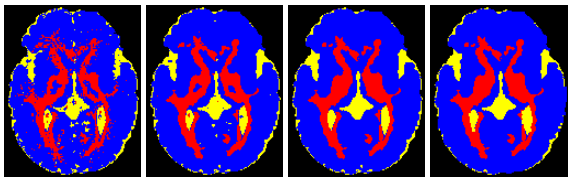

(a) (b) (c) (d)

Fig. 3. Applying pairwise (b), and higher order MGRF models (c) on a brain image (a)The 3D pairwise MGRF (b) corrected some of the erroneous parts in WM (red), GM (blue), and CSF (yellow). Results were better refined using 3D higher order MGRF(c). Ground truth image is shown in (d). Color map is used for visualization purposes.

2.3. Adaptive Shape Model

To enhance the segmentation accuracy, expected shapes of each brain label are constrained with an adaptive probabilistic shape prior. To create the shape database, a training set of images, collected for different subjects, are co-aligned by 3D affine transformations with 12 degrees of freedom (3 for the 3D translation, 3 for the 3D rotation, 3 for the 3D scaling, and 3 for the 3D shearing) in a way that maximizes their mutual Information [24]. The shape prior is a spatially variant independent random field of region labels for the co-aligned data:

$$P_{\mathrm{sp}}(\mathbf{m}) = \prod_{(x,y,z)\in \mathrm{R}} p_{\mathrm{sp}:x,y,z}(m_{x,y,z}) \tag{6}$$

where $p_{\mathrm{sp}:x,y,z}(l)$ is the voxel-wise empirical probabilities for each brain label $l \in \mathbf{L}$. For each input MR data to be segmented, the shape prior is constructed by an adaptive process guided by the visual appearance features of the input MRI data. First, the input subject is aligned with the database. Then, the normalized cross correlation similarity coefficient is used to select the subject from the shape database that has the best match with the input subject (i.e., highest similarity). The selected subject is then used as a reference prototype to co-align the input subject using the 3D affine transformation described above. A 3D window is then initialized for each voxel, where search for voxels with corresponding grey level values in all training images of equalized intensities is conducted. This search process plays the major role in creating label probabilities of the brain voxels. The framework is summarized in Algorithm 1, where the details of the proposed shape model are outlined in (steps 1, 2). The approach is also illustrated in Fig. 1.

Algorithm 1 Steps for the proposed segmentation approach

1. Preprocessing:
   (a) Use the developed automated approach [25, 26] to remove the skull from T1-weighted MR brain images, then construct the shape database through a co-alignment of the biased corrected training brains (both grey scale and manually segmented).
2. Create shape prior probability:
   (a) Align the test subject with the shape database.
   (b) Use normalized cross correlation to measure the similarity between the aligned test subject and each subject in the shape database, and choose the database subject that has the highest similarity to act as the reference in the registration process.
   (c) For each voxel in the test subject, calculate its shape prior probability according to the following steps:
      i. Use the transformation matrix T from (2) to transform each voxel to the reference domain.
      ii. Construct a 3D window with initial size of $N_{1i} \times N_{2i} \times N_{3i}$.
      iii. Search inside the window for voxels with corresponding grey level in all training data sets, where intensities of all training images are equalized.
      iv. If needed, increase the window size and redo the search until a non-empty result is found or maximum window size is reached.
      v. If maximum window size is reached and no result is found, increase the tolerance of grey level values and get back to step ii.
      vi. Create labels probabilities based on the relative occurrence of each label from the search results.
3. Start the segmentation process:
   (a) Approximate the marginal intensity distribution $P(\mathbf{g})$ of the T1-weighted MR brain image using an LCDG with four dominant modes.
   (b) Form an initial region map $\mathbf{m}$ using the marginal estimated density and prior shape of each brain label.
   (c) Find the Gibbs potentials for the MGRF model (for pairwise and higher-order cliques) from the initial map $\mathbf{m}$.
   (d) Improve $\mathbf{m}$ using the voxel-wise Iterative Conditional Mode (ICM) algorithm [27].

3. EXPERIMENTAL RESULTS AND CONCLUSIONS

To measure the robustness and performance of the proposed approach, the method is applied to T1-weighted infant MR brain data sets obtained from the Infant Brain Imaging Study (IBIS) [28]. MR data was acquired at 3T, voxel size of $1\times1\times1$ mm^3, and consists

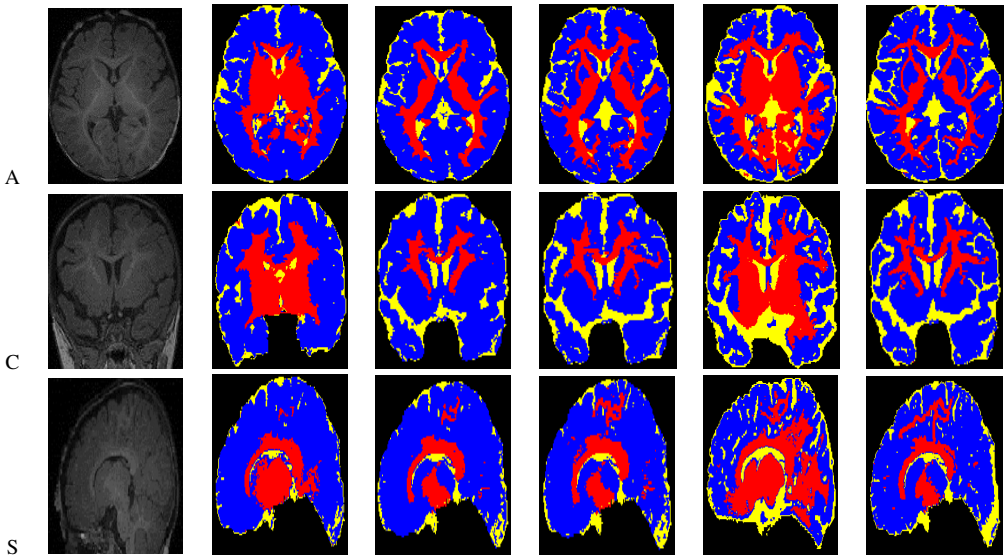

Fig. 4. Comparative Segmentation results. Segmentation is performed in 3D and the results are projected onto 2D axial (A), coronal (C), and sagittal (S) planes for visualization. (a) 2D profile of the original infant MRIs, (b) Applying the intensity model alone after skull stripping of (a).(c)Segmentation with intensity and spatial models. (d) Final segmentation results using intensity, spatial, and shape models (e) iBEAT segmentation results. (f) Ground truth of (a).WM, GM, and CSF are shown in red, blue, and yellow respectively.

of T1- and T2-weighted MR images of infants scanned at approximately 6 months old.

The ultimate goal of the proposed method is to separate infant MR brain images into four classes: WM, GM, CSF, and other brain tissue. Sample segmentation results using the proposed approach are shown in Fig. 4. The framework begins by removing the skull using an automated approach [25]. Using the intensity model, section 2.1, alone results in high rate of false positive findings, Fig. 4(b), therefore, the adaptive shape prior is co-guided by both a first-order visual appearance descriptor and the 3D spatial relationships between the region labels to segment each label. The classified brain structures using our method are demonstrated in Fig. 4. Fig. 4(c) shows results when integrating the spatial model with intensity. Fig. 4(d) shows the final segmentation after integrating shape with the former 2 models.

The proposed method was validated on forty 6-month-old subjects using leave-one-out approach, and evaluated with their manually segmented ground truth created by an MR expert. The performance of the proposed segmentation framework was evaluated using three performance metrics: (*i*) the Dice similarity coefficient (DSC) [29] that measures the overlap with ground truth, (*ii*) the 95-percentile modified Hausdorff distance (MHD) [30], where Hausdorff distance calculates the maximum distance of the segmented set to the nearest point in ground truth, and (*iii*) the absolute brain volume difference (ABVD) which measures the percentage of volume difference between ground truth and segmented data. Metrics were computed by comparing the ground truth segmentation to results from the proposed approach. As demonstrated in Table 4, the DSC for segmentation of the WM, GM, and the CSF are 94.7±1.53%, 93.86±0.13%, and 94.58±0.44%, respectively, which confirms the high accuracy of the proposed segmentation technique despite validating with the IBIS database which is known to be very challenging.

The proposed approach is compared against the software package presented in [31] named iBEAT for infant brain segmentation, Fig. 4(e). Segmentation accuracies for the two methods using the DSC, MHD, and ABVD are summarized in Table 1. These results document a significant improvement in accuracy for the proposed approach compared to one of the state-of-the-art- methods using a statistical paired t-test for the three performance metrics. In addition to the accuracy, the average time to segment an infant brain subject using the proposed approach is less than a minute (the algorithm is written in C++ and GPU), whereas it takes around 60 minutes using iBEAT. In conclusion, the proposed approach shows that an integration of a higher-order MGRF spatial model with first-order visual appearance features is a promising approach for guiding an adaptive shape model to segment T1-weighted infant brain MRIs. Thanks to an ongoing collaboration between our group and the IBIS group, there are plans to integrate the proposed approach into a framework that focuses on diagnosing autism in infants. The proposed framework will be integrated with other methodologies to explore features in GM and WM regions in order to differentiate autistic and control infant brains. As mentioned before, accuracy of segmentation would play a vital role in subsequent stages such as feature extraction from segmented brain surfaces.

Table 1. Accuracy of our approach vs. iBEAT using DSC(%), MHD, ABVD(%). Metrics are represented as Mean± Standard Deviation.

	WM		GM		CSF	
Metric	Ours	iBEAT	Ours	iBEAT	Ours	iBEAT
DSC	94.7±1.53	73.3±1.27	93.86±0.13	81.6±3.5	94.58±0.44	79.65±1.38
p-value		0.0001		0.0001		0.0001
MHD	7.3±1.23	18.27±1.53	3.5±0.24	23.3±0.52	4.35±1.1	27.23±1.43
p-value		0.0001		0.0001		0.0001
ABVD	3.17±1.73	37.94±0.61	1.62±1.24	34.46±0.18	1.9±0.114	21.07±0.98
p-value		0.0001		0.0001		0.0001

4. REFERENCES

[1] M. A. Balafar, A. R. Ramli, A. Saripan, and S. Mashohor, "Review of brain MRI segmentation methods," *Artificial Intelligence Review*, vol. 33, no. 3, pp. 261–274, 2010.

[2] A. Elnakib, G. Gimelfarb, J. S. Suri, and A. El-Baz, "Medical image segmentation: a brief survey," in *Multi Modality State-of-the-Art Medical Image Segmentation and Registration Methodologies*, pp. 1–39. Springer, 2011.

[3] N. Weisenfeld and S. K. Warfield, "Automatic segmentation of newborn brain MRI," *Neuroimage*, vol. 47, no. 2, pp. 564–572, 2009.

[4] H. Xue, L. Srinivasan, S. Jiang, M. Rutherford, A. Edwards, D. Rueckert, and J. Hajanl, "Automatic segmentation and reconstruction of the cortex from neonatal MRI," *Neuroimage*, vol. 38, no. 3, pp. 461–477, 2007.

[5] A. U. Mewes et al., "Regional brain development in serial magnetic resonance imaging of low-risk preterm infants," *Pediatrics*, vol. 118, no. 1, pp. 23–33, 2006.

[6] A. Barkovich, "Magnetic resonance techniques in the assessment of myelin and myelination," *Journal of inherited metabolic disease*, vol. 28, no. 3, pp. 311–343, 2005.

[7] A. Ortiz, J. M. Grriz, J. Ramirez, and D. Salas-Gonzalez, "MR brain image segmentation by growing hierarchical SOM and probability clustering," *Electronics Letters*, vol. 47, no. 10, pp. 585–586, 2011.

[8] A. Alansary, A. Soliman, F. Khalifa, A. Elnakib, M. Mostapha, M. Nitzken, M. F. Casanova, and A. El-Baz, "MAP–based framework for segmentation of mr brain images based on visual appearance and prior shape," *MIDAS Journal [online]. Available: http://hdl.handle.net/10380/3440*, 2013.

[9] L. Wang, Y. Chen, X. Pan, X. Hong, and D. Xia, "Level set segmentation of brain magnetic resonance images based on local Gaussian distribution fitting energy," *J. Neurosci. Methods*, vol. 188, no. 2, pp. 316–325, 2010.

[10] S. Bourouis and K. Hamrouni, "3D segmentation of MRI brain using level set and unsupervised classification," *Int. J. Image. Graph.*, vol. 10, no. 01, pp. 135–154, 2010.

[11] J.-P. Morin, C. Desrosiers, and L. Duong, "Atlas-based segmentation of brain magnetic resonance imaging using random walks," in *Computer Vision and Pattern Recognition Workshops (CVPRW'12)*, 2012, pp. 44–49.

[12] C. Ledig, R. Wolz, P. Aljabar, J. Lotjonen, R. A. Heckemann, A. Hammers, and D. Rueckert, "Multi-class brain segmentation using atlas propagation and em-based refinement," in *proceedings of IEEE International Symposium on Biomedical Imaging (ISBI)*, 2012, pp. 896–899.

[13] P. Anbeek, K. L. Vincken, F. Groenendaal, A. Koeman, M. J. Van Osch, and J. Van der Grond, "Probabilistic brain tissue segmentation in neonatal magnetic resonance imaging," *Pediatric Research*, vol. 63, no. 2, pp. 158–163, 2008.

[14] L. Wang, F. Shi, G. Li, W. Lin, J. H. Gilmore, and D. Shen, "Integration of Sparse Multi-modality Representation and Geometrical Constraint for Isointense Infant Brain Segmentation," in *Medical Image Computing and Computer-Assisted Intervention (MICCAI)*, pp. 703–710. 2013.

[15] L. Wang, Y. Gao, F. Shi, G. Li, J. H. Gilmore, W. Lin, and D. Shen, "Links: Learning-based multi-source integration framework for segmentation of infant brain image," in *MICCAI workshop on Medical Computer Vision*, 2014.

[16] L. Wang, F. Shi, P. T. Yap, W. Lin, J. H. Gilmore, and D. Shen, "Longitudinally guided level sets for consistent tissue segmentation of neonates," *Human Brain Mapping*, vol. 34, no. 4, pp. 956–972, 2013.

[17] F. Shi, Y. Fan, S. Tang, J. H. Gilmore, W. Lin, and D. Shen, "Neonatal brain image segmentation in longitudinal MRI studies," *Neuroimage*, vol. 49, no. 1, pp. 391–400, 2010.

[18] M. Altaye, S. K. Holland, M. Wilke, and C. Gaser, "Infant brain probability templates for MRI segmentation and normalization," *Neuroimage*, vol. 43, no. 4, pp. 721–730, 2008.

[19] Z. Song, S. P. Awate, D. J. Licht, and J. C. Gee, "Clinical neonatal brain mri segmentation using adaptive nonparametric data models and intensity-based markov priors," in *Medical Image Computing and Computer-Assisted Intervention (MICCAI)*, pp. 883–890. 2007.

[20] Z. Song, N. Tustison, B. Avants, and J. Gee, "Adaptive graph cuts with tissue priors for brain MRI segmentation," in *In proceedings of IEEE International Symposium on Biomedecial Imaging (ISBI)*, 2006, pp. 762–765.

[21] A. El-Baz, A. Elnakib, F. Khalifa, M. A. El-Ghar, P. McClure, A. Soliman, and G. Gimel'farb, "Precise segmentation of 3-D magnetic resonance angiography," *IEEE Transaction on Biomedical Engineering*, vol. 59, no. 7, pp. 2019–2029, 2012.

[22] A. El-Baz and G. Gimel'farb, "EM–based approximation of empirical distributions with linear combinations of discrete Gaussians," in *proceedings of IEEE International Conference on Image Processing (ICIP'07)*, San Antonio, Texas, USA, September 16–19, 2007.

[23] A. Farag, A. El-Baz, and G. Gimel'farb, "Precise segmentation of multimodal images," *IEEE Transactions on Image Processing*, vol. 15, no. 4, pp. 952–968, 2006.

[24] P. A. Viola and W. M. Wells III, "Alignment by maximization of mutual information," *International Journal of Computer Vision*, vol. 24, no. 2, pp. 137–154, 1997.

[25] A. Alansary, A. Soliman, M. Nitzken, F. Khalifa, A. Elnakib, M. Mostapha, M. F. Casanova, and A. El-Baz, "An integrated geometrical and stochastic approach for accurate infant brain extraction," in *In proceedings of International Conference on Image Processing (ICIP'14)*, 2014, pp. 3542–3546.

[26] A. Alansary, M. Ismail, A. Soliman, F. Khalifa, M. Nitzken, A. Elnakib, M. Mostapha, A. Black, K. Stinebruner, M. F. Casanova, J. M. Zurada, and A. El-Baz, "Infant brain extraction using BET and refinement using LCDG and MGRF models," *IEEE Journal of Biomedical and Health Informatics*, 2015, In Press.

[27] J. Besag, "On the statistical analysis of dirty pictures," *Journal or Royal Statistics Society: Series B*, vol. 48, no. 3, pp. 259–302, 1986.

[28] H. C. Hazlett, H. Gu, R. C. McKinstry, D. W. Shaw, K. N. Botteron, S. R. Dager, M. Styner, C. Vachet, G. Gerig, S. J. Paterson, et al., "Brain volume findings in 6-month-old infants at high familial risk for autism," *American Journal of Psychiatry*, vol. 169, no. 6, pp. 601–608, 2012.

[29] L. Dice, "Measures of the amount of ecologic association between species," *Ecology*, vol. 26, pp. 297–302, 1945.

[30] G. Gerig, M. Jomier, and M. Chakos, "Valmet: A new validation tool for assessing and improving 3D object segmentation," in *Medical Image Computing and Computer-Assisted Intervention (MICCAI)*, 2001, pp. 516–523.

[31] D. Yakang, F. Shi, L. Wang, G. Wu, and D. Shen, ""iBEAT: a toolbox for infant brain magnetic resonance image processing," *Neuroinformatics*, vol. 11, no. 2, pp. 211–225, 2013.